ACS OMEGA

http://pubs.acs.org/journal/acsodf

Article

Anisotropic Wooden Electromechanical Transduction Devices Enhanced by TEMPO Oxidization and PDMS

Bei Jiang, Meilin Li, Shuoang Cao, Zining Wang, Lijun Huang, Xinyi Song, Yuanqiao Zhang, and Quanping Yuan*

Cite This: *ACS Omega* 2023, 8, 3945−3955

Read Online

ACCESS | Metrics & More | Article Recommendations | Supporting Information

ABSTRACT: In order to increase the number and contact probability of electric dipole on cellulose, acid and alkali treatment was employed to extract hemicellulose and lignin from original wood to gain a highly oriented cellulose frame. The combined means with 2,2,6,6-tetramethylpiperidine-1-oxyl−NaBr−NaClO oxidation and impregnation of PDMS with compression was subsequently used to enhance its mechanical performance and electromechanical conversion. The assembled wooden electromechanical device (10 mm × 10 mm × 1 mm) exhibits the maximum open-circuit voltage (V_{OC}) of 11.75 V and short-circuit current (I_{SC}) of 211.01 nA as stepped by foot. It can be sliced to fabricate a flexible sensor with high sensitivity displaying V_{OC} of 2.88 V and I_{SC} of 210.09 nA under the tapped state. Its highly oriented wood fiber makes it display significant anisotropy in terms of mechanical and electromechanical performance for multidirectional sense. This strategy will exactly provide reference for developing other high-performance piezoelectric devices.

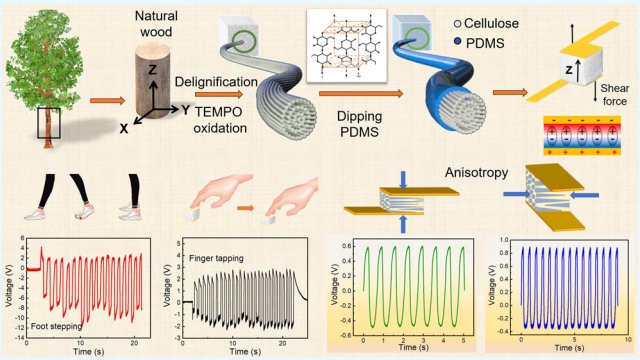

INTRODUCTION

Mechanical energy widely exists in the surrounding environment in various forms. Electromechanical devices, such as piezoelectric generators and triboelectric generators, can effectively convert mechanical energy into electrical energy, which attracted extensive attention in the fields of energy harvesters.[1,2] Various kinds of materials have been developed to fabricate the electromechanical devices.

As for triboelectric generators, its friction film mainly focused on the metal material (such as Al).[3] In order to improve its corrosion resistance and operation stability, many corrosion-resistant polymers had been developed for triboelectric generators. The triboelectric generators based on polydimethyl-siloxane (PDMS) and polyamide (PA)[4−6] displayed the super stability and high electromechanical efficiency.

In terms of piezoelectric generators, barium titanate ($BaTiO_3$) and lead zirconate titanate (PZT) with high piezoelectric coefficients have been mainly employed as the main piezoelectric elements, but their brittleness limits their application in flexible sensors and piezoelectric generators. A flexible piezoelectric polymer (such as polyvinylidene fluoride) with high piezoelectric coefficient, high mechanical strength, and flexibility can be perfectly used in most workplaces.[1]

Currently, developing renewable electromechanical devices with high flexibility and conversion performance has been a challenge. Recently, natural carbohydrate polymers such as paper-based materials,[7] lignocellulose,[8,9] and wood fiber derivatives[10−12] have been increasingly used to prepare generators, which promotes the development of an environmentally friendly generator.[13,14] Cellulose nanomaterials have attracted extensive attention for their sustainability and biocompatibility.[15,16] The unique mechanical properties and easy surface chemical modification make it widely used in triboelectric generators. Triboelectric generators with a cellulose nanofibril film as the top electrode can produce open-circuit voltage (V_{OC}) and short-circuit current (I_{SC}) up to 30 V and 90 μA, respectively.[17] The sensitivity of piezoelectric films prepared from CNFs ranged from 4.7 to 6.4 pC/N.[18] The facts prove the great potential of cellulose in the field of electromechanical conversion.

As the main source of cellulose, natural wood with unique mechanical properties and easy surface chemical modification provides conditions for its application in electromechanical conversion. The uniaxial orientation and monocline symmetry of cellulose crystals in wood fibers make it have certain piezoelectric properties.[19,20] In addition, under the action of

Received: October 13, 2022
Accepted: December 27, 2022
Published: January 20, 2023

https://doi.org/10.1021/acsomega.2c06607
ACS Omega 2023, 8, 3945−3955

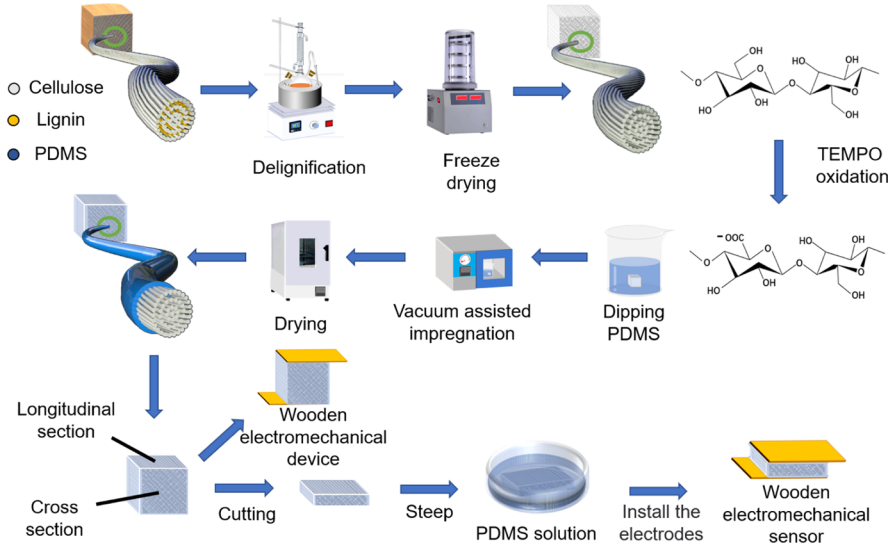

Figure 1. Preparation process and schematic diagram for the PWE, electromechanical conversion device, and sensor.

external forces, wood will also generate internal friction electricity, which has great potential in renewable electromechanical devices.[21,22] The piezoelectric modulus of conventional wood is about 1/20 of the quartz crystal.[20,23] The maximum output power density of the triboelectric generator prepared from pine wood reached 158.2 mW/m^2.[24] However, wood has low electrical properties because its cell wall contains lignin and hemicellulose, which have low crystallinity and affect its piezoelectric output.[25] In order to increase the contact probability of dipole, biological, chemical, and mechanical processing means were employed to extract hemicellulose and lignin from wood to gain a highly oriented cellulose frame, which has high crystallinity and elasticity. Its maximum output V_{OC} and I_{SC} was up to 0.69 V and 7.1 nA, respectively, which is 85 times more than that generated by natural balsa wood (0.0081 V).[25] Importantly, the output effect of wooden electromechanical devices is derived from both triboelectric and piezoelectric properties, even it is targeted to be assemble as self-powered sensors.[16,25]

The wooden porous material (WPM) formed by removing lignin and hemicellulose has high compressibility and contact probability of crystallization zones. The resulted porous structure increases its electric charge, which can improve its output performance.[16,26] What is more, the side groups of polymers are related to the states of charge transfer,[27] functional group modification is commonly used to improve the electrical conversion performance.

In this work, we propose a preparation method to develop an environmentally friendly wooden electromechanical conversion device with anisotropy and excellent resilience. The WPMs with a highly oriented cellulose frame were first gained by carrying out the acid and alkali treatment to remove hemicellulose and lignin from original wood, and then, the combined means with 2,2,6,6-tetramethylpiperidine-1-oxyl (TEMPO)−NaBr−NaClO oxidation and impregnation with PDMS suffered a certain of compression was used to enhance its mechanical performance and electromechanical conversion. The influence of TEMPO oxidation with various dosages of sodium hypochlorite and various compression rates on the morphology, structure, and the combination with PDMS of WPMs, as well as the mechanical performance, thermal stability, and electromechanical conversion performance of the assembled devices and sensors were mainly discussed. The oxidization can provide more electric dipoles and increase its surface charge for the piezoelectric and triboelectric response. A hypothesis that there is an obvious synergistic effect for the TEMPO oxidation and impregnation of PDMS to enhance the mechanical performance and electromechanical conversion of the wood material had been put forward. The presented method of the wooden electromechanical device will provide reference for the development of this kind of devices and sensor.

EXPERIMENTAL SECTION

Materials. Balsa wood (air-dry density: 0.15−0.2 g/cm^3) was used. Sodium chlorite ($NaClO_2$, ≥80.0%) was purchased from Damao Chemical Reagent Factory (Tianjin, China). Sodium hydroxide (NaOH, ≥96.0%) was used. Glacial acetic acid (GAA, ≥99.5%) was produced by Cologne Chemicals Co. Ltd. (Chengdu, China). The TEMPO radical was purchased from Aladdin Chemistry Co. Ltd (Shanghai, China). Sodium bromide (NaBr, ≥99.0%), sodium hypochlorite solution (NaClO), and available chlorine ≥10.0% were made by Jinshan Chemical Reagent Co. Ltd. (Chengdu, China). Ethyl alcohol (EtOH), mass fraction ≥99.7%, AR, was purchased from Fuyu Fine Chemicals Co. Ltd. (Tianjin, China). Hydrochloric acid (HCl), concentration from 36.0 to 38.0%, AR, was obtained from Cologne Chemicals Co. Ltd. (Chengdu, China). Silver epoxy adhesive, type of CW2400, was purchased from ITW Chemtronics Inc. A copper foil, thickness of 0.02 mm, was used.

Experiments. *Fabrication and TEMPO Oxidation of the WPM.* First, balsa wood at the angle of 40−60° between the growth rings and the horizontal plane on the transverse section was cut into square blocks with the dimension of 10 mm × 10 mm × 10 mm (Figure 1). Its initial weight was measured and recorded after being dried for 24 h at 100 °C. It was then placed in a treating fluid mixed with $NaClO_2$ (3 wt%) at 95 °C for 6 h, and the pH was regulated as 3.5 by adding GAA. After the first treatment, the residual chemicals were removed by soaking in deionized water for 10 min. Subsequently, the sample was immersed in 6 wt % NaOH solution at 95 °C for 6 h to further remove lignin. The resulting sample was rinsed

https://doi.org/10.1021/acsomega.2c06607
ACS Omega 2023, 8, 3945−3955

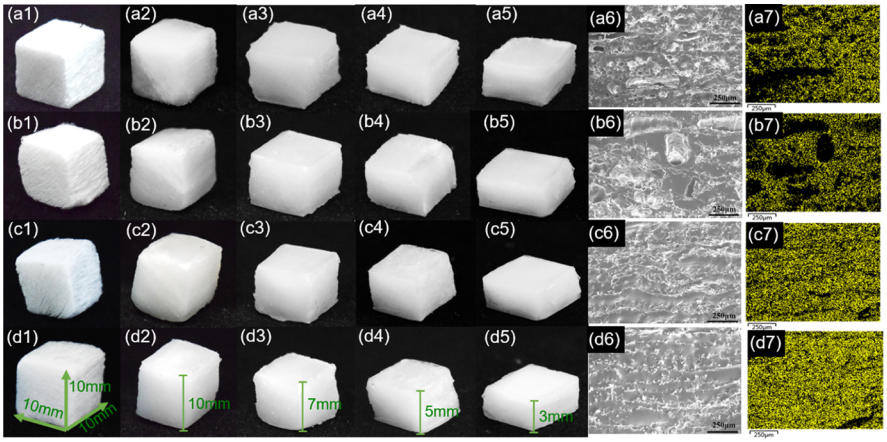

Figure 2. Appearance of different wood samples: (a1) WPM, (a2) PWE, (a3) PWE at a compression rate of 30, 50 (a4), and 70% (a5). (b1) OWPM-0.2, (b2) OPWE-0.2, and (b3) OPWE-0.2 at a compression rate of 30, 50 (b4), and 70% (b5). (c1) OWPM-0.5, (c2) OPWE-0.5, and (c3) OPWE-0.5 at a compression rate of 30, 50 (c4), and 70% (c5). (d1) OWPM-1.0, (d2) OPWE-1.0, and (d3) OPWE-1.0 at a compression rate of 30, 50 (d4), and 70% (d5). SEM images (cross sections) of OPWE and PWE: (a6) PWE, (b6) OPWE-0.2, (c6) OPWE-0.5, and (d6) OPWE-1.0. Si element distribution (cross section) of OPWE and PWE: (a7) PWE, (b7) OPWE-0.2, (c7) OPWE-0.5, and (d7) OPWE-1.0.

with deionized water and stood in aqueous ethanol solution for 48 h. The solution was changed every 24 h and then rinsed and stood in distilled water for 24 h to remove the remaining chemicals. After that the WPM can be obtained by cooling the samples at −40 °C for 2 h and then drying them with a freeze dryer for 12 h. The WPM prepared in the abovementioned steps was mixed with the system of TEMPO (0.032 g), sodium bromide (0.32 g), sodium hypochlorite (0.2, 0.5, and 1.0 mmol/g), and 50 mL of deionized water at room temperature. The pH of the system was maintained at 10.5 by dropping NaOH (0.1 mol/L) and HCl (0.1 mol/L) solution. The reaction was completed when pH of the solution was maintained at 10.5 for 15 min without adding NaOH. The resulting sample was soaked in anhydrous ethanol and stirred gently and then washed to remove the chemical agent to the neutral state. Finally, the TEMPO oxidized WPMs (OWPMs) were obtained. The specific preparation process can be seen in Figure 1. Moreover, Figure S1 shows the catalytic oxidation of the cellulose C6 aldehyde group to C6 carboxyl group by TEMPO. NaClO is the main oxidant in this process. It first forms NaBrO with NaBr, and then, NaBrO oxidizes TEMPO to nitrosonium, which oxidizes the primary alcohol hydroxyl to the aldehyde group (intermediate) and finally generates the carboxyl group.[28,29]

Preparation of PDMS/Wooden Elastomer. The OWPMs were dipped in the PDMS solution (ratio between the base and curing agent was 10:1) with the help of vacuum-impregnated process for 2 h and then were cured at 60 °C for 24 h. The OWPMs prepared with various contents of sodium hypochlorite were seen as OWPMs-0 (0 mmol/g), OWPMs-0.2 (0.2 mmol/g), OWPMs-0.5 (0.5 mmol/g), and OWPMs-1.0 (1.0 mmol/g). The corresponding PWEs were denoted as PWE-0, OPWE-0.2, OPWE-0.5, and OPWE-1.0, respectively. Before curing, the dipped samples were compressed to various degrees (compression rates of 30, 50, and 70%).

Preparation of the Wooden Electromechanical Devices and Sensors. The conductive copper foil was cut into 10 mm × 10 mm size, then was pasted on the longitudinal section on both sides of the elastomer, and dried at 60 °C for 6 h to obtain the electromechanical device (shown in Figure 1). In order to demonstrate its application potential in flexible electromechanical devices, a slice with thickness of 1.5 mm parallel to the longitudinal direction of wooden fiber was cut from the elastomer as a piezoelectric layer. Subsequently, it was immersed in PDMS solution and kept under vacuum for 30 min. After taking it out, the conductive copper foil (10 mm × 10 mm) was pasted on two surface sides of the piezoelectric layer and then was hot-pressed under 1 MPa at 60 °C for 6 h. Finally, the PDMS on its surface was cured completely to obtain thin wooden piezoelectric sensors.

Measurement Methods. The samples were coated with Pt/Pd nanoparticles by a CCCU.010 Safematic HPMA53 Metal sputtering coater, and their section morphology was characterized by scanning electron microscopy (SEM, SU8020, HITACHI, Japan). Fourier transform infrared spectra (FTIR, IRTracer-100, Shimadzu Corp., Japan) in the wavenumber range of 400−4000 cm^{-1} were recorded to analyze chemical properties before and after treatment, as well as X-ray photoelectron spectrometry (XPS, Thermo Fisher Scientific Inc., USA). The X-ray diffraction (XRD) patterns of the samples before and after lignin removal were recorded with an X-ray diffractometer (Bruker D8Advance, SMARTLAB 3K, Rigaku Corp., Japan) using a Cu Kα radiation at a scanning rate of 7°/min. The diffraction angle ranged from 5 to 50°. A Dtg-60 (H) differential thermogravimetric analyzer (DTA-TG, Shimadzu Corp., Japan) was used to analyze the thermal stability under the protection of nitrogen in the range of 36−600 °C with the heating rate of 10 °C/min. A Universal material testing machine (8801, Instron, UK) was used to test the stress−strain curves in the compression process. The charge acquisition system (KR6259-FNG-SYS) was used to test the output performance. The controlled external forces (45, 55, and 65 N) were applied to excite the devices and sensors by a linear motor (B01-37) in the frequency of 1.5 Hz, as well as electrometer (Keithley 6514, Tektronix, USA) with the matched software was used to record the output V_{OC} and I_{SC}.

RESULTS AND DISCUSSION

Structure and Morphology of the Wooden Electromechanical Conversion Materials. As shown in Figure 1, hemicellulose and lignin and cellulose are wound together to form fiber bundles, which can be linked with each other via

https://doi.org/10.1021/acsomega.2c06607
ACS Omega 2023, 8, 3945−3955

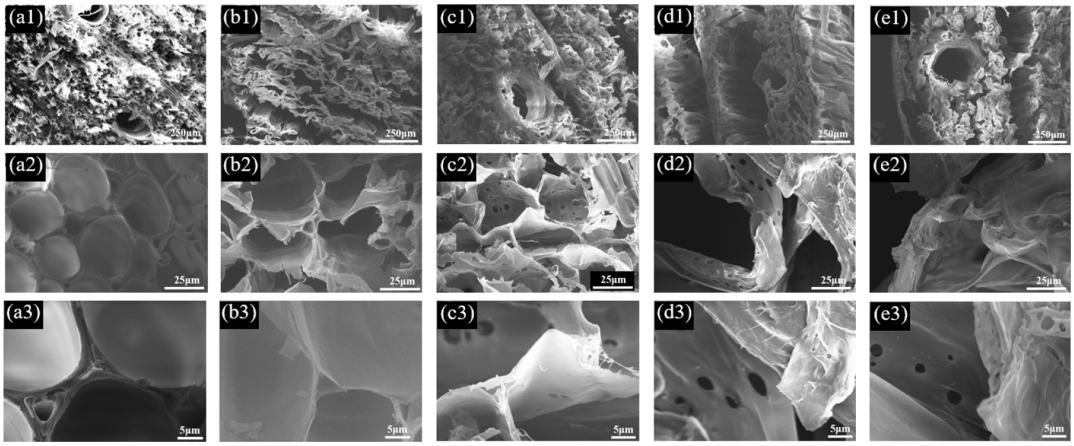

Figure 3. SEM morphology structure of different wood samples. (a) Natural wood and (b) WPM. OWPM prepared with various amounts of sodium hypochlorite: (c) 0.2, (d) 0.5, and (e) 1.0 mmol/g.

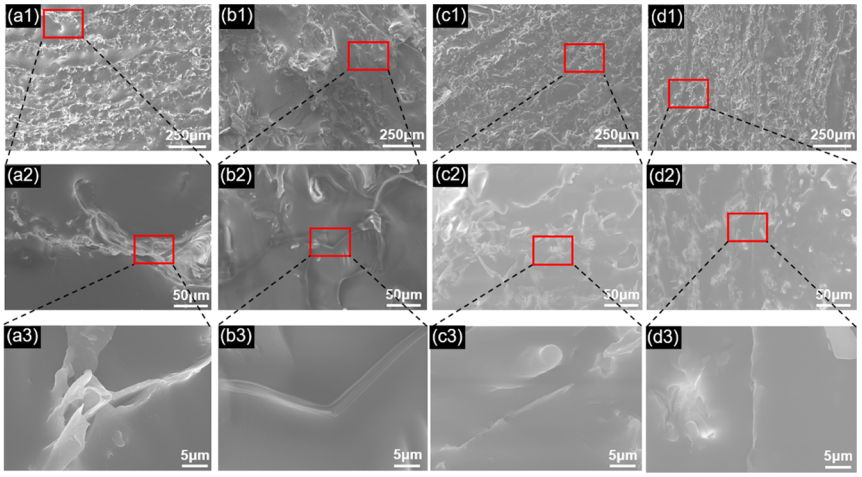

Figure 4. SEM analysis on the cross section of OPWE-1.0 at different compression degrees: (a) un-compressed and (b) 30, (c) 50, and (d) 70% compression ratio.

covalent bonds and act as physical barriers.[30,31] The white WPM in Figure 2 was obtained by preparing from balsa wood (Figure 2a1), which indicates that the dark lignin had been removed and the colorless polysaccharides had been left behind.[32]

It was found from Figure 3a1−a3,b1−b3 that after the acid and alkali treatment, there is an obvious aperture gap existing in the intercellular layer and the honeycomb cell cavities at the cross section, similar to a porous layer structure of sponge. In addition, with the increase of TEMPO oxidation degree, some cell cavity of OWPM was destroyed, and the thin cell wall is decomposed to form pores (Figure 3c1−c3,d1−d3,e1−e3). The appearance of the WPM tends to be fluffier (Figure 2a1,b1,c1,d1). As shown in Figure 3c1−c3,d1−d3,e1−e3, after further oxidation on the WPM, its cross section presents a layered stack structure with thinner cell walls and larger gaps. The phenomenon is attributed to the fact that primary alcohol hydroxyl groups on fibers were selectively oxidized into corresponding carboxyl groups during TEMPO oxidation, which increases the electrostatic repulsion between the fibers.[33,34]

As can be seen in Figure 2b2,c2,d2, the appearance of PWE at different oxidation degrees shows that the wood fibers can be well coated by PDMS, which has sufficiently permeated in the OWPM, while most wood fibers were not coated by PDMS in the un-oxidized WPM, presenting pure white wood fibers (Figure 2a2). As shown in the SEM morphology at the cross section in Figure 2a6,b6,c6,d6, when the oxidation degree of the WPM tends to be higher, there is a more compact structure at the cross section, which can be further confirmed from the more uniform and compact distribution of the Si element (seen in Figure 2a7−d7) on that. In particular, OPWE-1.0 exhibits the most even and compact structure for the bundle and homogeneous pore in the OWPM prepared with 1.0 mmol/g sodium hypochlorite (seen in Figure 4), which has been evenly filled by PDMS. After the oxidation, cellulose in the porous material has been oxidized to endow with a fluffy porous structure allowing exposure of more active groups,[33] which favors the permeation of PDMS and the binding to fibers.

Figure 2a2−a5,b2−b5,c2−c5,d2−d5 shows that the distribution of the filled PDMS in PWE and OPWEs become more homogeneous with the increase of compression degree. As seen in Figure 4, fibers in the compressed elastomer were more closely bound to PDMS. The cell cavity, the dissociated wood cell wall, and intercellular layer were further filled by PDMS. At the same time, the proportion of unfilled cell cavities on its surface decreased significantly, as well as that no obvious fiber

https://doi.org/10.1021/acsomega.2c06607
ACS Omega 2023, 8, 3945−3955

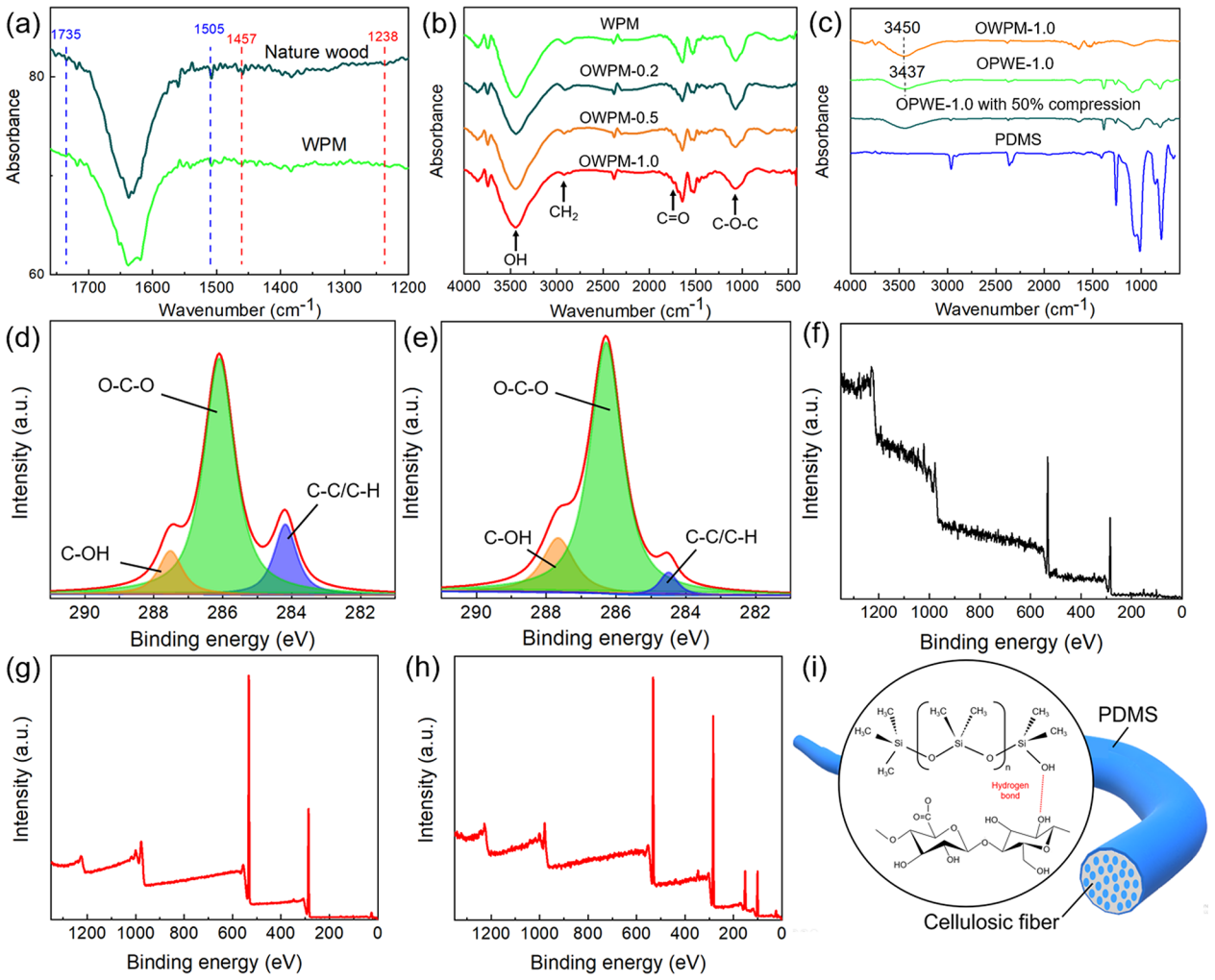

Figure 5. FTIR spectra of WPM (a), OWPM (b), and PWE (c), OWPM-1.0, OPWE-1.0, OPWE-1.0 with 50% compression rate and PDMS. XPS analysis on different wooden samples: (d,f) WPM, (e,g) OWPM-1.0, and (h) OPWE-1.0. (i) Schematic diagram for the bonding between PDMS and cellulose fiber.

shape and wood texture structure can be seen. In addition, SEM and Si element analyses (Figures 4 and S2) at the cross section of OPWE-1.0 at the compression rate of 50% show the more uniform distribution of the Si element, further indicating the compression effect that there should be a closer combination existing between the wood fiber and PDMS.

Chemical Properties and Phase Structure of the Wooden Elastomer. FTIR analysis in Figure 5a confirms that characteristic peaks at 1238 and 1457 cm^{-1} attributing to benzene ring carbon skeleton vibration of lignin almost disappear after the chemical treatment.[35] Meanwhile, the c-tensile vibration peak (xylan acetyl group) at 1505 cm^{-1} of the WPM was sharply weakened. The strength of the peak at 1735 cm^{-1} corresponding to hemicellulose decreased distinctly. These results show that lignin and hemicellulose are removed substantially after the chemical treatment.[36]

As shown the FTIR spectra in Figure 5b, there is a broad band around 3450 cm^{-1} corresponding to the −OH stretching vibration in both un-oxidized and oxidized porous materials. Moreover, a new peak appears at 1720 cm^{-1} attributing to C═O stretching vibration, which indicates the successful conversion of D-glucose hydroxyl to carboxyl.[37] Meanwhile, with the increase of oxidation degree, the peak strength becomes stronger for the higher content of the conversed carboxyl. In the XPS analysis in Figure 5d,e,g, there are C3 peak at 287.5 eV, C2 peak at 286 eV, and C1 peak at 284 eV, corresponding to C═O, C−O, and C−C structures in the WPM, respectively.[38,39] By fitting the relative contents of various C elements, the proportion of C2 increased from 73.70 to 79.60% after oxidation. The proportion of C3 is 16.5%, which indicates the further oxidation occurring in the WPM (15.9%). The actual oxidation is also confirmed from that the ratio of oxygen to carbon (calculation based on the XPS analysis results in Figure 5f,g) was elevated from 70.61% (WPM) to 78.62% (OWPM-1.0).

There is a new binding energy peak in XPS spectra in Figure 5h, which appears at 101 eV and corresponds to the Si element of the PWE. This fact also proves that PDMS has been successfully impregnated into the WPM. It can be found in Figure 5c that the OWPM impregnated with PDMS shows new peaks at 1261 and 799 cm^{-1} (symmetrical bending and oscillation of CH_3 in Si−CH_3) as well as new peaks at 1092 and 1020 cm^{-1} (asymmetric symmetry stretching of Si−O−Si).[40,41] At the same time, the peak position of O−H stretching vibration shifts slightly to low wave direction (move from 3450 to 3437 cm^{-1}) after the impregnation, indicating that there may be the hydrogen bond (Figure 5i) between PDMS and cellulose.[42]

https://doi.org/10.1021/acsomega.2c06607
ACS Omega 2023, 8, 3945−3955

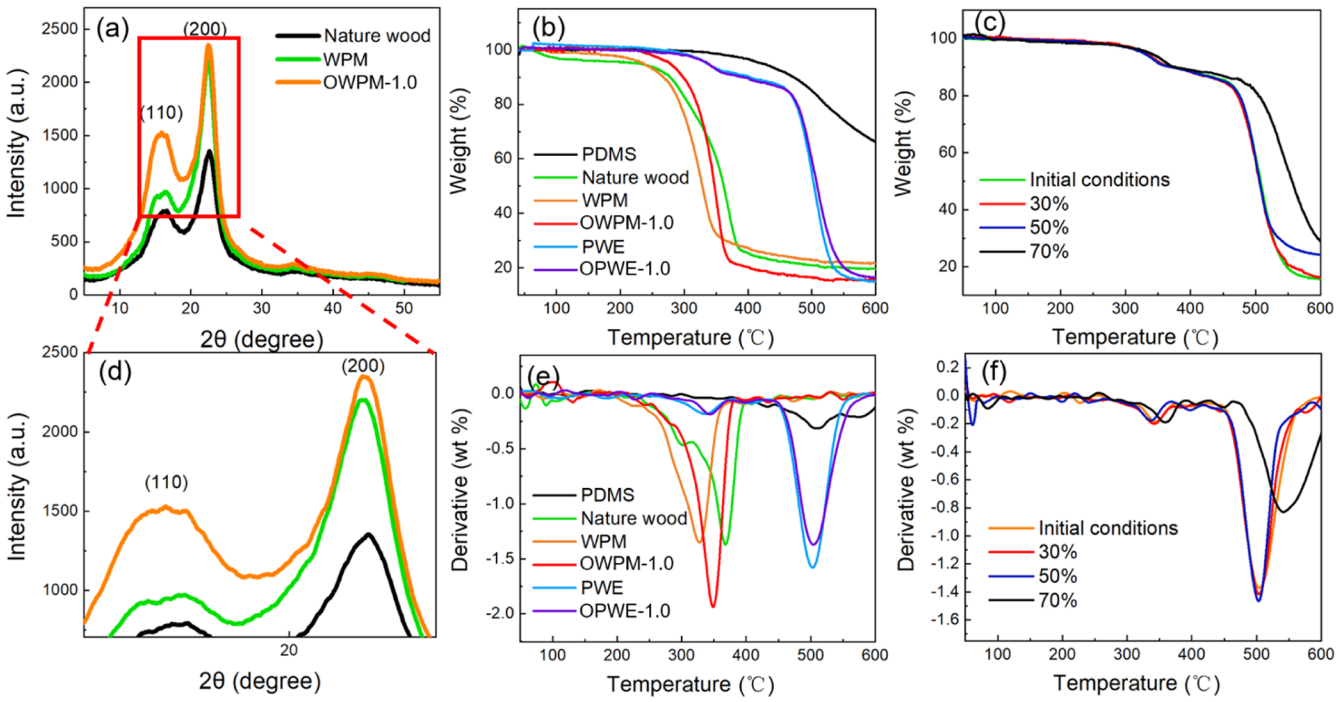

Figure 6. (a) XRD analysis of different samples. TG analysis of different samples: (b) PDMS, nature wood, WPM, OWPM-1.0, PWE, and OPWE-1.0. (c) TG analysis of different degrees of compression. (d) XRD analysis based on (a). (e) DTG analysis of different samples: PDMS, nature wood, WPM, OWPM-1.0, PWE, and OPWE-1.0. (f) DTG analysis of OPWE-1.0 at different degrees of compression.

Generally, the diffraction peaks of cellulose I (110) and (200) exist at 16−17° and 22−23° (Figure 6a), respectively.[43] After the chemical treatment, the crystal structure of cellulose in the WPM did not change and the relative strength of the diffraction peaks of wooded materials and wood sponges increased slightly due to the partial removal of lignin and hemicellulose. The peak position shifts slightly to the right, indicating that the crystal plane spacing of cellulose I in the WPM decreased and the density of the docking between atoms increased. When an external force was applied to it, the electric dipole in the cellulose I lattice shifts or redirects, resulting in the piezoelectricity effect.[25]

As shown in Figure 6a,d, the XRD pattern of wood fiber has almost no change before and after TEMPO oxidation, indicating that during the oxidation process of TEMPO, the carboxyl group only exists on the surface of the crystalline or amorphous cellulose area and inside the amorphous area.[33,44] With the use of oxidants, the crystallinity of cellulose increases, because the oxidation takes place in the amorphous area and part of the crystalline area of the cellulose, so the crystallinity will increase at the beginning of the reaction,[45] which is beneficial to the increase of the piezoelectric output of wood porous materials.

As shown in Figure 6b, nature wood and WPM have shown an obvious mass loss at 225−400 °C. After impregnated with PDMS, its thermal stability was obviously enhanced with the main mass loss range of 360−600 °C. In addition, the thermal stability of the OPWE-1.0 is slightly higher than that of the PWE. It can be seen from DTG analysis in Figure 6e that the maximum thermal decomposition temperature of PWE is significantly higher than that of the WPM. This fact suggests a stable bond existing between the WPM and PDMS. Compared with PWE, OPWE-1.0 displays the slightly higher maximum thermal decomposition temperature in the first (about 343 °C) and second (about 504 °C) thermal decomposition peak, indicating that the combination between the oxidized fiber and PDMS is more stable.[41] In Figure 6c, with the increase of compression degree, the mass residual rate is gradually enlarged. In particular, there is highest maximum thermal decomposition temperature in OPWE-1.0 with a compression rate of 70% (Figure 6f). Therefore, the compression has enhanced the combination between PDMS and wood fiber as well as the orientation of the wood fiber, thus elevating its thermal stability.

Compressive Mechanical Properties of the PWE and OPWE. The horizontal compression test was carried out to develop the application potential of the PWE in pressure sensing and mainly discuss its mechanical stability and elasticity. In the PWE, the integrity of the layered structure of the WPM was greatly maintained, thereby improving the compressibility.[42] When the WPM suffers the compressive pressure of 33.77 kPa, the strain reached 40% (Figure S3). After it was impregnated with PDMS, the highest compression ratio only reached 30% under 389.60 kPa; otherwise, the damage will occur, but they display the higher recovery ratio and recovery rate (Figure S4). The damage is mainly attributed to that the binding between the fiber and PDMS is not tight enough, as well as the PDMS did not sufficiently permeate the porous material. Thus, the damage occurs in the area of wood fiber without PDMS under the loading pressure. However, after the OWPM-1.0 impregnated with PDMS (OPWE-1.0) was compressed to a certain degree, it can suffer the higher compression ratio. In particular, OPWE-1.0 prepared with the compression ratio of 70% can bear the compressive pressure as high as 0.93 MPa with the high strain of 50% without damage (Figure S3). The enhanced performance is mainly attributed to the enhanced combination between PDMS and wood fiber after the compression process, which was also confirmed from the abovementioned SEM, FTIR, and XPS analyses. In addition, the PDMS layer outside surface can also act as a

https://doi.org/10.1021/acsomega.2c06607
ACS Omega 2023, 8, 3945−3955

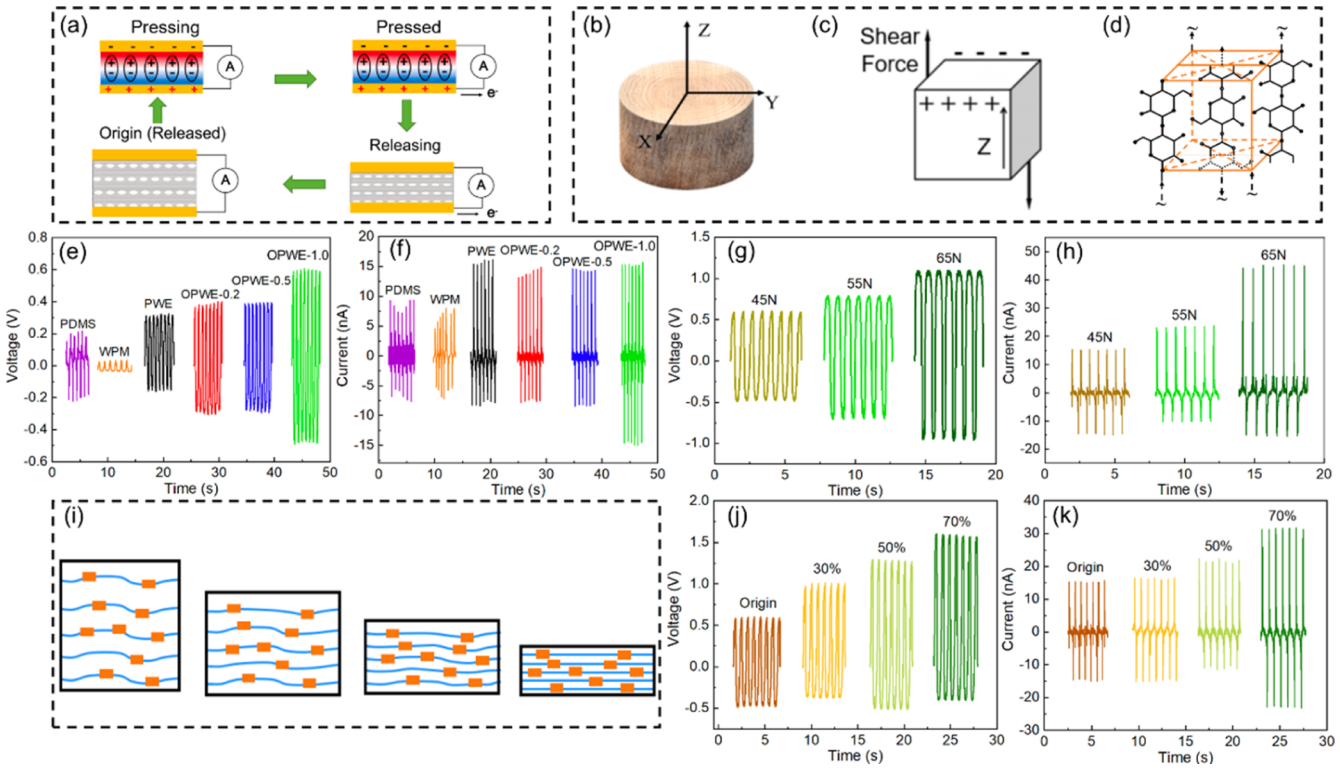

Figure 7. (a) Principle of the piezoelectric effect. Schematic diagram of (b) wood, (c) piezoelectric polarization produced in wood, and (d) monoclinic crystal structure of cellulose. Comparison of the piezoelectric output of different samples: (e) V_{OC} and (f) I_{SC}. Comparison of the piezoelectric output of OPWE-1.0 under different forces: (g) V_{OC} and (h) I_{SC}. (i) Schematic diagram for orientation of the cellulose crystal under various compression degrees. Comparison of the piezoelectric output of OPWE-1.0 prepared with different compression degrees: (j) V_{OC} and (k) I_{SC}.

buffer layer to protect the elastomer from direct impacts, thus improving the mechanical properties and durability. Because the OPWEs remain the anisotropic property of natural wood, it also exhibits a high strength at longitudinal compression without a high compression rate similar to the horizontal compression.

Electromechanical Conversion Performance of the Wooden Electromechanical Devices. The piezoelectric effect of wood is due to the noncentral symmetry of cellulose monoclinic crystal structure and its dipole orientation under existing force.[46] As seen in Figure 7a, the deformation of the WPM will induce the displacement of the cellulose crystal during the compression process and then it causes electric polarization of the cellulose crystal, which will generate a piezoelectric potential field between the upper and lower electrodes, thus forming a current through the external circuit. As the applied force is released, an electrical signal in reverse is generated. This continuous application of force and the release of pressure produce an alternating output signal.[47] The piezoelectric effect mechanism in wood can be observed, as illustrated in Figure 7b–d. A square wood plate cut at an angle of 45° to the grain direction was commonly used to measure the piezoelectric performance.[20] As shown in Figure 7e,f, the electromechanical output (V_{OC} and I_{SC}) of the WPM after the removal of lignin was 0.03 V and 7.14 nA under the loading force of 13.3 kPa, which is about 80 times than that (0.089 nA) of the natural wood.[25] The presence of lignin in wood results in a small deformation of cellulose under action stress. It also obstructs the electron transfer generated from the cellulose crystal. These facts result in the low piezoelectric properties of natural wood.[25]

In the pure PDMS layer, these electrical signals may be due to electrostatic charges induced from triboelectricity occurring at the interface between the copper electrode and the PDMS. The piezoelectric output V_{OC} of OPWE-1.0 was 0.60 V, which is significantly higher than that of the pure WPM (0.03 V) shown in Figure 7 and OWPM-1.0 (0.05 V) shown in Figure S5.

The presence of PDMS in PWE not only makes it exhibit permanent electric dipole moment but also form the hydrogen bond between the −OH group generated by the chain break of the Si−O−Si group of PDMS and the oxygen atom on the cellulose, which significantly increases the density of electric dipole.[42,48−50] Therefore, under the same compressive stress, PWE shows higher piezoelectric properties than pure PDMS and WPM (Figure 7e,f). Oxidized cellulose has good absorption capacity, and so, PDMS is more evenly distributed and completely filled in the OWPM. It may lead to a denser structure connected by hydrogen bonds in the OWPM impregnated with PDMS, and so, the density of its electric dipole is greater.[42] Therefore, with the increase of oxidation degree, the piezoelectric output performance of the sample was further increased. In particular, OPWE-1.0 has a higher piezoelectric output V_{OC} of 0.60 V under 45 N (Video S1). The stability and reliability of OPWE-1.0 are evaluated by continuously applying and releasing cyclic compressive stresses. As shown in Figure S6, its output voltage signal performance has hardly decreased after 10,000 s of operation. As further increasing the loading force, V_{OC} and I_{SC} were further elevated to 1.09 V and 45.40 nA under the loading force of 65 N (Figure 7g,h).

https://doi.org/10.1021/acsomega.2c06607
ACS Omega 2023, 8, 3945−3955

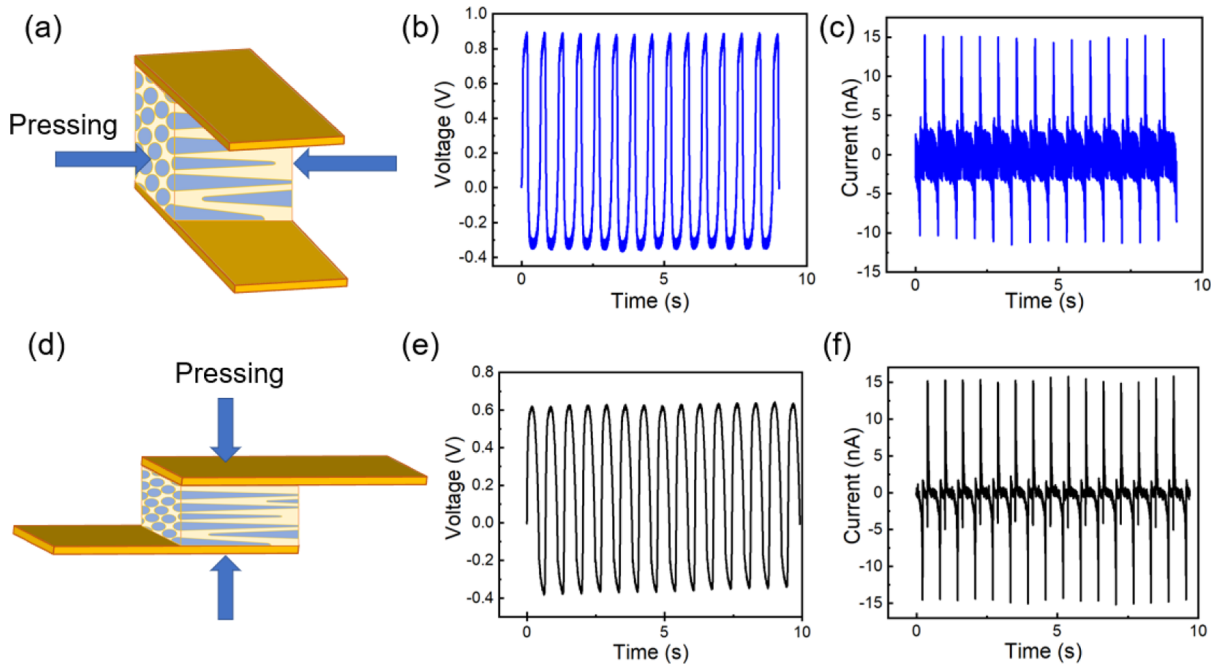

Figure 8. (a) Direction parallel to the fiber direction for applying pressure to the OPWE-1.0, (b) piezoelectric output of V_{OC} of (a), (c) piezoelectric output of I_{SC} of (a), (d) direction perpendicular to the fiber direction for applying pressure to the OPWE-1.0, (e) piezoelectric output of V_{OC} of the sample (d), and (f) piezoelectric output of I_{SC} of the sample (d).

After the OPWE-1.0 was compressed in the preparation process, the density and orientation of the cellulose crystal were strengthened (Figure 7i), and the PDMS will further flow and permeate the interval among the cellulose and its surface, which helps the electron transfer generated from the cellulose crystal and the stress transfer for the piezoelectric response. As seen in Figure 7j,k, under the same loading force of 45 N, the piezoelectric output performance exhibits an ascending trend with the increase of the compression ratio. The V_{OC} and I_{SC} of the original OPWE-1.0 are 0.60 V and 15.25 nA, respectively, while they are 1.29 V and 21.36 nA under the compression ratio of 50%, as well as 1.58 V and 31.26 nA under the higher compression ratio of 70%.

The wooden electromechanical devices developed in this work retain the anisotropic spatial structure of natural wood, in which the highly oriented distribution of wood fiber makes it display anisotropy in terms of mechanical properties (Figure S3) and electromechanical properties (Figure 8). When the force applied direction is parallel to the fiber direction (Figure 8a), output V_{OC} and I_{SC} are 0.89 V and 15.24 nA (Figure 8b,c), respectively, while they are 0.60 V and 15.25 nA (Figure 8e,f) at the direction perpendicular to the fiber direction (Figure 8d), under the exciting force of 45 N. There is a difference of output performance between the two directions. There is a possible existence of triboelectricity in the structure shown in Figure 8a for the tiny movement between the electrode and surface of the elastomer when the measurement was carried out.

Application Performance of the Wooden Electromechanical Devices. A thin wooden elastomer was sliced to fabricate flexible thin wooden electromechanical sensors (the dimensions are 10 mm × 10 mm × 1 mm) by spinning PDMS layers on both sides to assemble electrodes (as shown in Figure 1). The PDMS layer on the elastomer can enhance the output performance by preventing charge leakage and transferring compressive stress efficiently. The thin structure endows it with better flexibility. Generally, piezoelectricity exists in the wood fiber as well as triboelectricity exists between PDMS and wood fibers, so as to realize the synchronous conversion under the same mechanical energy. As shown in Figure 9, the thin piezoelectric sensor can be directly used to detect the pressure and deformation signals. It can be internally installed in the shoe sole for the movement monitoring or the energy harvesting (Figure 9a,b). When repeatedly stepping on the wooden electromechanical sensor with your foot (Video S2), the output V_{OC} displays an instantaneous minimum of 1.07 V and the maximum of 11.75 V, accompanied with an instantaneous minimum I_{SC} of 84.87 nA and the maximum of 211.01 nA (as shown in Figure 9c,e).

It can be seen in Figure 9d,f, when tapping on the wooden electromechanical sensor with finger (Video S3), it shows the instantaneous minimum V_{OC} of 1.81 V (the maximum V_{OC} is 2.88 V) and the minimum I_{SC} of 108.16 nA (the maximum I_{SC} is 210.09 nA). Compared with previously reported wooden piezoelectric materials,[25] the presented wooden electromechanical sensors in our work have considerable piezoelectric performance. Furthermore, the WPM is a natural polymer from a wide range of sources, and its biocompatibility makes it possible to be developed as a sensor in medical facilities or other special fields. As for its highly oriented fiber structure with high elasticity, the sensor has high flexibility and excellent mechanical stability, which can be applied in the working environment under high-strength force. Moreover, there is a higher sensitivity at the force loading direction perpendicular to the cross section of the wooden electromechanical sensors for its higher compression strength, while there is relatively low sensitivity at the direction perpendicular to the longitudinal section for the higher compressibility. Consequently, it has the potential application in the multidirectional sensing, as well as exhibits excellent mechanical strength along the fiber direction, which can work as the support accompanied by the sensing and monitoring performance. Since electrode polarization is

https://doi.org/10.1021/acsomega.2c06607
ACS Omega 2023, 8, 3945−3955

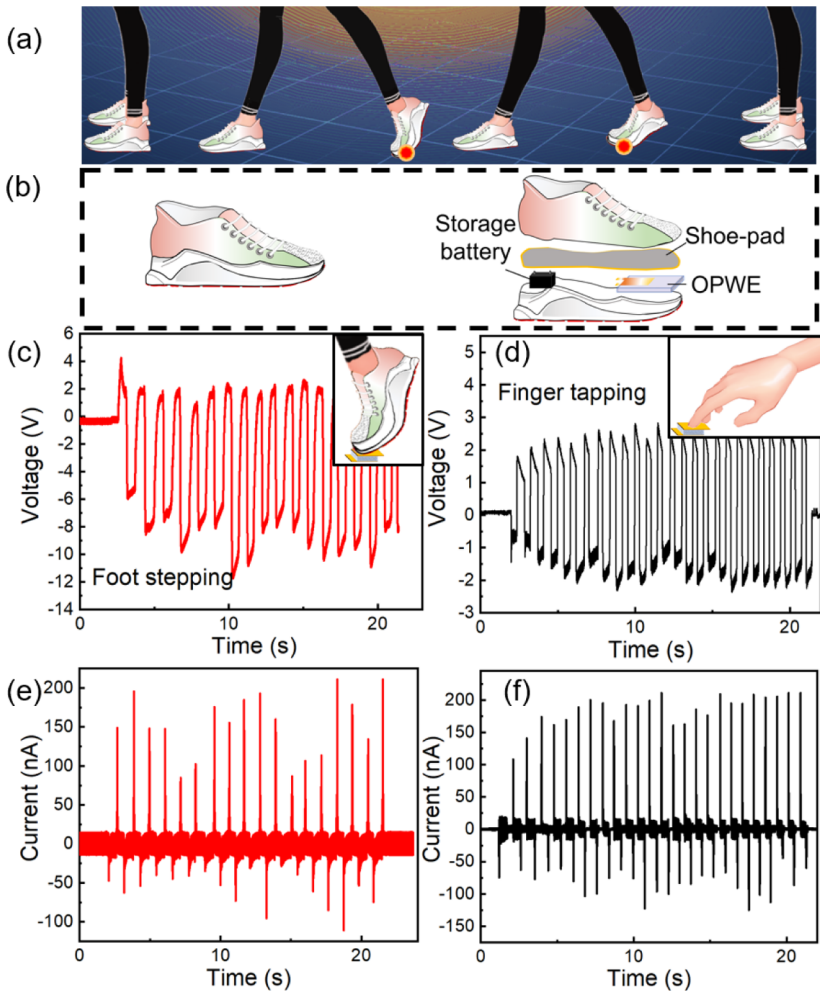

Figure 9. Schematic diagram of the application (a) and assembly (b) of the energy harvesting device and sensor in walking. Motion-induced output V_{OC}: (c) foot tramping and (d) finger tapping. I_{SC}: (e) foot tramping and (f) finger tapping.

not required, the process is simple and highly efficient. It is expected that it can be applied into wooden furniture, such as wooden tables or floors, enabling energy harvesting functions within the building.

CONCLUSIONS

In this paper, a highly elastic wooden electromechanical conversion device with anisotropic properties was obtained from natural wood by carrying out a series of processing means involving the acid and alkali treatment, TEMPO-oxidation, and vacuum impregnation of PDMS, followed by a certain amount of compression. The chemical treatment created a more porous structure and active group (hydroxyl and carboxyl groups) in the porous material, which has synergistically contributed to the addition of electric dipole for electromechanical conversion, complete impregnation of PDMS, and tight combination with PDMS. The immersed PDMS increases the stress transfer and mechanical properties, which has enhanced the mechanical compression resilience and the repeatability of its electromechanical output. Under the loading force of 45 N, the V_{OC} and I_{SC} of the original OPWE-1.0 are 0.60 V and 15.25 nA, respectively, while that are elevated to 1.58 V and 31.26 nA under the compression ratio of 70%.

Specially, it has obvious anisotropic compression and electromechanical performance at various forces loaded in the direction perpendicular to the longitudinal section and cross section of the wooden electromechanical conversion device, which can be used for the multidirectional sense at the same time.

Furthermore, it can be also sliced to fabricate flexible thin wooden electromechanical sensors with high sensitivity, displaying the instantaneous maximum V_{OC} of 2.88 V and the maximum I_{SC} of 210.09 nA under the pressure of a finger.

Thus, the developed wooden electromechanical conversion devices have the exact potential for the fields of energy harvesters and electromechanical sensor. The oriented porous template effect of the WPM and the presented method of the device will exactly provide reference for the structure optimization of similar electromechanical conversion devices and sensor.

ASSOCIATED CONTENT

Supporting Information

The Supporting Information is available free of charge at https://pubs.acs.org/doi/10.1021/acsomega.2c06607.

Voc of the OPWE-1.0 electromechanical device (MP4)

Voc of flexible wooden sensor as stepped by foot (MP4)

Voc of flexible wooden sensor as tapped by finger (MP4)

https://doi.org/10.1021/acsomega.2c06607
ACS Omega 2023, 8, 3945−3955

Additional results, including morphology structure, schematic diagram for the anisotropic mechanical properties, stress−strain curves, resilience test, and piezoelectric output, as well as the video on the output V_{OC} of the OPWE-1.0 electromechanical device, and flexible wooden sensor as stepped by foot and tapped by finger (PDF)

AUTHOR INFORMATION

Corresponding Author

Quanping Yuan − *School of Resources, Environment and Materials and MOE Key Laboratory of New Processing Technology for Non-Ferrous Metals and Materials & Guangxi Key Laboratory of Processing for Non-Ferrous Metals and Featured Materials, Guangxi University, Nanning 530004, China*; orcid.org/0000-0001-9376-9246; Email: yuanquanping@gxu.edu.cn

Authors

Bei Jiang − *School of Resources, Environment and Materials and MOE Key Laboratory of New Processing Technology for Non-Ferrous Metals and Materials & Guangxi Key Laboratory of Processing for Non-Ferrous Metals and Featured Materials, Guangxi University, Nanning 530004, China*

Meilin Li − *School of Resources, Environment and Materials and MOE Key Laboratory of New Processing Technology for Non-Ferrous Metals and Materials & Guangxi Key Laboratory of Processing for Non-Ferrous Metals and Featured Materials, Guangxi University, Nanning 530004, China*

Shuoang Cao − *School of Resources, Environment and Materials and MOE Key Laboratory of New Processing Technology for Non-Ferrous Metals and Materials & Guangxi Key Laboratory of Processing for Non-Ferrous Metals and Featured Materials, Guangxi University, Nanning 530004, China*

Zining Wang − *School of Resources, Environment and Materials and MOE Key Laboratory of New Processing Technology for Non-Ferrous Metals and Materials & Guangxi Key Laboratory of Processing for Non-Ferrous Metals and Featured Materials, Guangxi University, Nanning 530004, China*

Lijun Huang − *School of Resources, Environment and Materials and MOE Key Laboratory of New Processing Technology for Non-Ferrous Metals and Materials & Guangxi Key Laboratory of Processing for Non-Ferrous Metals and Featured Materials, Guangxi University, Nanning 530004, China*

Xinyi Song − *School of Resources, Environment and Materials and MOE Key Laboratory of New Processing Technology for Non-Ferrous Metals and Materials & Guangxi Key Laboratory of Processing for Non-Ferrous Metals and Featured Materials, Guangxi University, Nanning 530004, China*

Yuanqiao Zhang − *School of Resources, Environment and Materials and MOE Key Laboratory of New Processing Technology for Non-Ferrous Metals and Materials & Guangxi Key Laboratory of Processing for Non-Ferrous Metals and Featured Materials, Guangxi University, Nanning 530004, China*

Complete contact information is available at: https://pubs.acs.org/10.1021/acsomega.2c06607

Author Contributions

The manuscript was written through contributions of all authors. All pictures and videos in the manuscript are taken by all authors. All authors have given approval to the final version of the manuscript.

Notes

The authors declare no competing financial interest.

ACKNOWLEDGMENTS

The authors thank the financial support from the National Natural Science Foundation of China (project no.: 32071695).

REFERENCES

(1) Kim, S. H.; Park, S. J.; Cho, C. Y.; Kang, H. S.; Sohn, E. H.; Park, I. J.; Ha, J. W.; Lee, S. G. Preparation and electroactive phase adjustment of Ag-doped poly(vinylidene fluoride) (PVDF) films. *RSC Adv.* **2019**, *9*, 40286−40291.

(2) Lin, Y. F.; Song, J.; Ding, Y.; Lu, S. Y.; Wang, Z. L. Piezoelectric nanogenerator using CdS nanowires. *Appl. Phys. Lett.* **2008**, *92*, 022105.

(3) Yang, W. Q.; Chen, J.; Zhu, G.; Yang, J.; Bai, P.; Su, Y. J.; Jing, Q. S.; Cao, X.; Wang, Z. L. Harvesting energy from the natural vibration of human walking. *ACS Nano* **2013**, *7*, 11317−11324.

(4) Lee, K. Y.; Chun, J.; Lee, J.-H.; Kim, K. N.; Kang, N.-R.; Kim, J. Y.; Kim, M. H.; Shin, K.-S.; Gupta, M. K.; Baik, J. M.; Kim, S.-W. Hydrophobic sponge structure-based triboelectric nanogenerator. *Adv. Mater.* **2014**, *26*, 5037−5042.

(5) Tofel, P.; Částková, K.; Říha, D.; Sobola, D.; Papež, N.; Kaštyl, J.; Ţălu, S.; Hadaš, Z. Triboelectric response of electrospun stratified PVDF and PA structures. *Nanomaterials* **2022**, *12*, 349.

(6) Liu, Z. Q.; Muhammad, M.; Cheng, L.; Xie, E. Q.; Han, W. H. Improved output performance of triboelectric nanogenerators based on polydimethylsiloxane composites by the capacitive effect of embedded carbon nanotubes. *Appl. Phys. Lett.* **2020**, *117*, 143903.

(7) Kim, H. S.; Li, Y.; Kim, J. Electro-mechanical behavior and direct piezoelectricity of cellulose electro-active paper. *Sensors Actuators A* **2008**, *147*, 304−309.

(8) Zhang, M.; Du, H. S.; Liu, K.; Nie, S. X.; Xu, T.; Zhang, X. Y.; Si, C. L. Fabrication and applications of cellulose-based nanogenerators. *Adv. Compos. Hybrid Mater.* **2021**, *4*, 865−884.

(9) Niu, Z. X.; Cheng, W. L.; Cao, M. L.; Wang, Q. X.; Wang, J. Q.; Han, Y. Z.; Long, G. P.; Han, G. Recent advances in cellulose-based flexible triboelectric nanogenerators. *Nano Energy* **2021**, *87*, 106175.

(10) Srither, S. R.; Shankar Rao, D. S.; Krishna Prasad, S. Triboelectric nanogenerator based on biocompatible and easily available polymer films. *ChemistrySelect* **2018**, *3*, 5055−5061.

(11) Bai, Z. Q.; Xu, Y. L.; Zhang, Z.; Zhu, J. J.; Gao, C.; Zhang, Y.; Jia, H.; Guo, J. S. Highly flexible, porous electroactive biocomposite as attractive tribopositive material for advancing high-performance triboelectric nanogenerator. *Nano Energy* **2020**, *75*, 104884.

(12) Bai, Z. Q.; Xu, Y. L.; Li, J. C.; Zhu, J. J.; Gao, C.; Zhang, Y.; Wang, J.; Guo, J. S. An eco-friendly porous nanocomposite fabric-based triboelectric nanogenerator for efficient energy harvesting and motion sensing. *ACS Appl. Mater. Interfaces* **2020**, *12*, 42880−42890.

(13) Lai, S. N.; Chang, C. K.; Yang, C. S.; Su, C. W.; Leu, C. M.; Chu, Y. H.; Sha, P. W.; Wu, J. M. Ultrasensitivity of self-powered wireless triboelectric vibration sensor for operating in underwater environment based on surface functionalization of rice husks. *Nano Energy* **2019**, *60*, 715−723.

(14) Wu, J. M.; Chang, C. K.; Chang, T. C. High-output current density of the triboelectric nanogenerator made from recycling rice husks. *Nano Energy* **2016**, *19*, 39−47.

(15) Li, M. C.; Wu, Q. L.; Moon, R. J.; Hubbe, M. A.; Bortner, M. J. Rheological aspects of cellulose nanomaterials: governing factors and emerging applications. *Adv. Mater.* **2021**, *33*, 2006052.

(16) Mi, H. Y.; Jing, X.; Zheng, Q. F.; Fang, L. M.; Huang, H. X.; Turng, L. S.; Gong, S. Q. High-performance flexible triboelectric nanogenerator based on porous aerogels and electrospun nanofibers for energy harvesting and sensitive self-powered sensing. *Nano Energy* **2018**, *48*, 327−336.
(17) Yao, C. H.; Hernandez, A.; Yu, Y. H.; Cai, Z. Y.; Wang, X. D. Triboelectric nanogenerators and power-boards from cellulose nanofibrils and recycled materials. *Nano Energy* **2016**, *30*, 103−108.
(18) Rajala, S.; Siponkoski, T.; Sarlin, E.; Mettänen, M.; Vuoriluoto, M.; Pammo, A.; Juuti, J.; Rojas, O. J.; Franssila, S.; Tuukkanen, S. Cellulose nanofibril film as a piezoelectric sensor material. *ACS Appl. Mater. Interfaces* **2016**, *8*, 15607−15614.
(19) Gardner, K. H.; Blackwell, J. The structure of native cellulose. *Biopolymers* **1974**, *13*, 1975−2001.
(20) Fukada, E. Piezoelectricity as a fundamental property of wood. *Wood Sci. Technol.* **1968**, *2*, 299−307.
(21) Bang, J.; Moon, I. K.; Jeon, Y. P.; Ki, B.; Oh, J. Fully wood-based green triboelectric nanogenerators. *Appl. Surf. Sci.* **2021**, *567*, 150806.
(22) Yu, Z. H.; Wang, Y. M.; Zheng, J. Q.; Xiang, Y.; Zhao, P.; Cui, J. Q.; Zhou, H. M.; Li, D. Q. Rapidly fabricated triboelectric nanogenerator employing insoluble and infusible biomass materials by fused deposition modeling. *Nano Energy* **2020**, *68*, 104382.
(23) Fukada, E. Piezoelectricity of wood. *J. Phys. Soc. Jpn.* **1955**, *10*, 149−154.
(24) Hao, S. F.; Jiao, J. Y.; Chen, Y. D.; Wang, Z. L.; Cao, X. Natural wood-based triboelectric nanogenerator as self-powered sensing for smart homes and floors. *Nano Energy* **2020**, *75*, 104957.
(25) Sun, J. G.; Guo, H. Y.; Ribera, J.; Wu, C. S.; Tu, K. K.; Binelli, M.; Panzarasa, G.; Schwarze, F. W. M. R.; Wang, ZL.; Burgert, I. Sustainable and biodegradable wood sponge piezoelectric nanogenerator for sensing and energy harvesting applications. *ACS Nano* **2020**, *14*, 14665−14674.
(26) Zhang, C. Y.; Lin, X. J.; Zhang, N.; Lu, Y. X.; Wu, Z. M.; Liu, G. L.; Nie, S. X. Chemically functionalized cellulose nanofibrils-based gear-like triboelectric nanogenerator for energy harvesting and sensing. *Nano Energy* **2019**, *66*, 104126.
(27) Lowell, J.; Rose-Innes, A. C. Contact electrification. *Adv. Phys.* **1980**, *29*, 947−1023.
(28) Saito, T.; Isogai, A. Introduction of aldehyde groups on surfaces of native cellulose fibers by TEMPO-mediated oxidation. *Colloids Surf. A* **2006**, *289*, 219−225.
(29) Iwamoto, S.; Kai, W.; Isogai, T.; Saito, T.; Isogai, A.; Iwata, T. Comparison study of TEMPO-analogous compounds on oxidation efficiency of wood cellulose for preparation of cellulose nanofibrils. *Polym. Degrad. Stab.* **2010**, *95*, 1394−1398.
(30) Chang, V. S.; Holtzapple, M. T. Fundamental factors affecting biomass enzymatic reactivity. *Appl. Biochem. Biotechnol.* **2000**, *84-86*, 5−38.
(31) Zhu, H. L.; Luo, W.; Ciesielski, P. N.; Fang, Z. Q.; Zhu, J. Y.; Henriksson, G.; Himmel, M. E.; Hu, L. B. Wood-derived materials for green electronics, biological devices, and energy applications. *ACS Chem. Rev.* **2016**, *116*, 9305−9374.
(32) Song, J. W.; Chen, C. J.; Yang, Z.; Kuang, Y. D.; Li, T.; Li, Y. J.; Huang, H.; Kierzewski, I.; Liu, B. Y.; He, S. M.; Gao, T. T.; Yuruker, S. U.; Gong, A.; Yang, B.; Hu, L. B. Highly compressible, anisotropic aerogel with aligned cellulose nanofibers. *ACS Nano* **2018**, *12*, 140−147.
(33) Besbes, I.; Alila, S.; Boufi, S. Nanofibrillated cellulose from TEMPO-oxidized eucalyptus fibres: effect of the carboxyl content. *Carbohydr. Polym.* **2011**, *84*, 975−983.
(34) Saito, T.; Nishiyama, Y.; Putaux, J. L.; Vignon, M.; Isogai, A. Homogeneous suspensions of individualized microfibrils from TEMPO-catalyzed oxidation of native cellulose. *Biomacromolecules* **2006**, *7*, 1687−1691.
(35) Lemaire, E.; Ayela, C.; Atli, A. Eco-friendly materials for large area piezoelectronics: self-oriented Rochelle salt in wood. *Smart Mater. Struct.* **2018**, *27*, 025005.
(36) Pandey, K. K. Study of the effect of photo-irradiation on the surface chemistry of wood. *Polym. Degrad. Stab.* **2005**, *90*, 9−20.
(37) Martínez-Salcedo, S. L.; Torres-Rendón, J. G.; García-Enriquez, S.; Anzaldo-Hernández, J.; Silva-Guzmán, J. A.; de Muniz, G. I. B.; Lomelí-Ramírez, M. G. Physicomechanical characterization of poly-(acrylic acid-co-acrylamide) hydrogels reinforced with TEMPO-oxidized blue agave cellulose nanofibers. *Fibers Polym.* **2022**, *23*, 1161−1170.
(38) Kolářová, K.; Vosmanská, V.; Rimpelová, S.; Švorčík, V. Effect of plasma treatment on cellulose fiber. *Cellulose* **2013**, *20*, 953−961.
(39) Chen, X.; Liu, L.; Luo, Z.; Shen, J.; Ni, Q.; Yao, J. Facile preparation of a cellulose based bioadsorbent modified by hPEI in heterogeneous system for high-efficiency removal of multiple types of dyes. *React. Funct. Polym.* **2018**, *125*, 77−83.
(40) Lancastre, J. J. H.; Fernandes, N.; Margaça, F. M. A.; Miranda Salvado, I. M. M.; Ferreira, L. M.; Falcão, A. N.; Casimiro, M. H. Study of PDMS conformation in PDMS-based hybrid materials prepared by gamma irradiation. *Radiat. Phys. Chem.* **2012**, *81*, 1336−1340.
(41) Yang, R.; Liang, Y. Y.; Hong, S.; Zuo, S. D.; Wu, Y. J.; Shi, J. T.; Cai, L. P.; Li, J. Z.; Mao, H. Y.; Ge, S. B.; Xia, C. L. Novel low-temperature chemical vapor deposition of hydrothermal delignified wood for hydrophobic property. *Polymers* **2020**, *12*, 1757.
(42) Zheng, Q. F.; Zhang, H. L.; Mi, H. Y.; Cai, Z. Y.; Ma, Z. Q.; Gong, S. Q. High-performance flexible piezoelectric nanogenerators consisting of porous cellulose nanofibril (CNF)/poly (dimethylsiloxane) (PDMS) aerogel films. *Nano Energy* **2016**, *26*, 504−512.
(43) Oun, A. A.; Rhim, J. W. Preparation and characterization of sodium carboxymethyl cellulose/cotton linter cellulose nanofibril composite films. *Carbohydr. Polym.* **2015**, *127*, 101−109.
(44) Saito, T.; Shibata, I.; Isogai, A.; Suguri, N.; Sumikawa, N. Distribution of carboxylate groups introduced into cotton linters by the TEMPO-mediated oxidation. *Carbohydr. Polym.* **2005**, *61*, 414−419.
(45) Saito, T.; Isogai, A. TEMPO-mediated oxidation of native cellulose. The effect of oxidation conditions on chemical and crystal structures of the water-insoluble fractions. *Biomacromolecules* **2004**, *5*, 1983−1989.
(46) Nakai, T.; Yamamoto, H.; Nakao, T.; Hamatake, M. Mechanical behavior of the crystalline region of wood and the piezoelectric response of wood in tension tests. *Wood Sci. Technol.* **2005**, *39*, 163−168.
(47) Zhu, G.; Wang, A. C.; Liu, Y.; Zhou, Y. S.; Wang, Z. L. Functional electrical stimulation by nanogenerator with 58 V output voltage. *Nano Lett.* **2012**, *12*, 3086−3090.
(48) Alam, M. M.; Mandal, D. Native cellulose microfiber-based hybrid piezoelectric generator for mechanical energy harvesting utility. *ACS Appl. Mater. Interfaces* **2016**, *8*, 1555−1558.
(49) Jana, S.; Garain, S.; Sen, S.; Mandal, D. The influence of hydrogen bonding on the dielectric constant and the piezoelectric energy harvesting performance of hydrated metal salt mediated PVDF films. *Phys. Chem. Chem. Phys.* **2015**, *17*, 17429−17436.
(50) Werling, K. A.; Griffin, M.; Hutchison, G. R.; Lambrecht, D. S. Piezoelectric hydrogen bonding: computational screening for a design rationale. *J. Phys. Chem. A* **2014**, *118*, 7404−7410.

https://doi.org/10.1021/acsomega.2c06607
ACS Omega 2023, 8, 3945−3955